

A General and Efficient Algorithm for the Likelihood of Diversification and Discrete-Trait Evolutionary Models

STILIANOS LOUCA^{1,2,*} AND MATTHEW W. PENNELL^{3,4}

¹Department of Biology, 1210 University of Oregon, Eugene, OR 97403, USA; ²Institute of Ecology and Evolution, 5289 University of Oregon, Eugene, OR 97403, USA; ³Biodiversity Research Centre, University of British Columbia, 2212 Main Mall, Vancouver, V6T1Z4 British Columbia, Canada; and

⁴Department of Zoology, University of British Columbia, 6270 University Blvd, Vancouver, V6T1Z4 British Columbia, Canada

*Correspondence to be sent to: Department of Biology, 1210 University of Oregon, Eugene, OR 97403, USA; E-mail: louca.research@gmail.com.

Received 15 January 2019; reviews returned 14 August 2019; accepted 15 August 2019

Associate Editor: Stephen Smith

Abstract.—As the size of phylogenetic trees and comparative data continue to grow and more complex models are developed to investigate the processes that gave rise to them, macroevolutionary analyses are becoming increasingly limited by computational requirements. Here, we introduce a novel algorithm, based on the “flow” of the differential equations that describe likelihoods along tree edges in backward time, to reduce redundancy in calculations and efficiently compute the likelihood of various macroevolutionary models. Our algorithm applies to several diversification models, including birth–death models and models that account for state- or time-dependent rates, as well as many commonly used models of discrete-trait evolution, and provides an alternative way to describe macroevolutionary model likelihoods. As a demonstration of our algorithm’s utility, we implemented it for a popular class of state-dependent diversification models—BiSSE, MuSSE, and their extensions to hidden-states. Our implementation is available through the R package *castor*. We show that, for these models, our algorithm is one or more orders of magnitude faster than existing implementations when applied to large phylogenies. Our algorithm thus enables the fitting of state-dependent diversification models to modern massive phylogenies with millions of tips and may lead to potentially similar computational improvements for many other macroevolutionary models. [Dynamical systems theory; extinction; flow; likelihood; macroevolution; speciation.]

There is a vast, and ever-growing, array of statistical models that can be fit to phylogenetic trees and comparative data to investigate the historical dynamics of diversification, trait evolution, and the interaction between the two (O’Meara 2012; Pennell and Harmon 2013; Morlon 2014; Ng and Smith 2014; Harmon 2018). These models have empowered researchers to move beyond summary statistics such as tree balance (Mooers and Heard 1997), toward explicitly quantifying the variation in speciation and extinction rates across the Tree of Life (Magallon and Sanderson 2001; Alfaro et al. 2009; Henao Diaz et al. 2019) and identifying the major drivers of this variation (Schluter and Pennell 2017; Wiens 2017). Concurrently, the scale of comparative data has also been growing tremendously. There are now phylogenetic trees for multiple groups that contain tens of thousands or even millions of lineages (Jetz et al. 2012; Zanne et al. 2014; Hinchliff et al. 2015; Thompson et al. 2017; Parks et al. 2018; Smith and Brown 2018)—though we are still far from having a comprehensive representation of the full Tree of Life (Mora et al. 2011; Hinchliff et al. 2015; Larsen et al. 2017). Similarly, large-scale efforts are underway to assemble trait information for many lineages, both multicellular (Cornwell et al. 2019) and microbial (Mendler et al. 2019).

Taken together, these developments provide tremendous opportunities for gaining new insights into macroevolutionary processes at unprecedented scales. However, as we show below, current computational procedures for fitting macroevolutionary models become practically unfeasible at the scale of modern megaphylogenies. This greatly limits the analyses conductible with existing models and restricts the

future development of even more complex models. For example, massive bacterial phylogenies could shed light on the role that the repeated loss and gain of metabolic functions, generally suspected to be dominated by horizontal gene transfer (David and Alm 2011; Polz et al. 2013; Hehemann et al. 2016), has had on bacterial diversification over geological time scales (Latysheva et al. 2012). Models for state-dependent speciation and extinction (Maddison et al. 2007; FitzJohn 2012; Goldberg and Igić 2012; Herrera-Alsina et al. 2019; Caetano et al. 2018) would be particularly suited for such an analysis, but are computationally too demanding to be applied at this scale.

To address these emerging challenges, we leverage results from dynamical systems theory, a well-established field in physics and mathematics (Meiss 2007), and develop a novel algorithm for computing the likelihood of a large class of models for diversification and trait evolution. Dynamical systems theory investigates the behavior of time-dependent systems (including their trajectories, equilibria, and stability), often described through differential equations analogous to the “equations of motion” in classical mechanics. Calculating the likelihood of macroevolutionary models often translates to calculating the solution of an equation of motion for a set of probabilities along a tree’s branches, in backward time. As we show below, basic tools from dynamical systems theory can thus be used to devise an algorithm for macroevolutionary likelihood calculations that can be orders of magnitude faster than existing approaches. Our work also highlights a previously unrecognized deep similarity between seemingly distinct classes of

methods; we anticipate that the recognition of this similarity will help spur the development of new types of models.

CLASSICAL APPROACHES FOR CALCULATING LIKELIHOODS OF MACROEVOLUTIONARY MODELS

Birth–death processes (Kendall 1948) have long been a pillar of macroevolutionary theory (Raup 1985), and following the pioneering work of Nee et al. (1994) researchers have routinely fit these models to phylogenetic data. While the simple, single-rate birth–death process has been extended to an impressive variety of models (Morlon 2014; Harmon 2018), these modifications broadly fall into three major classes. First, there may be variation in speciation and extinction rates through time (Rabosky et al. 2007; Morlon et al. 2011; Stadler 2011a); this includes models where the rates depend on another environmental variable (e.g., Condamine et al. 2013). Second, a phylogeny may be partitioned by clade into several rate classes (Alfaro et al. 2009; Rabosky 2014). And third, rates at each lineage may be associated with the current state of an evolving trait. The pioneering work of (Maddison et al., 2007) and their BiSSE (Binary State Speciation and Extinction) model triggered the development of a plethora of State-dependent Speciation and Extinction (SSE) models. For example, it is now possible to fit models where diversification rates vary with the state of a multistate character (MuSSE; FitzJohn et al. 2009), geographic area (GeoSSE; Goldberg et al. 2011), or quantitative character (QuaSSE; FitzJohn 2010), and character transitions may occur either along lineages (anagenetic transitions; FitzJohn et al. 2009) or during speciation events (cladogenetic transitions; Goldberg and Igić 2012; Magnuson-Ford and Otto 2012). More recently, SSE models have been extended to include hidden-states (Beaulieu and O’Meara 2016; Caetano et al. 2018; Herrera-Alsina et al. 2019), which has been demonstrated to greatly improve the applicability of SSE-type models (Caetano et al. 2018). These ways of introducing variation (by time, clade, or state) are not mutually exclusive (e.g., Rabosky and Glor 2010; Morlon et al. 2011; Cantalapiedra et al. 2014), nor are they exhaustive (e.g., Etienne and Haegeman 2012). Finally, some models merely describe the evolution of discrete characters along branches of a given phylogeny, that is, diversification and character evolution are assumed to have occurred independently (Pagel 1994; Lewis 2001).

Beneath this apparent variety of models lies a deep similarity. Indeed, the likelihood of all of these models can be computed by moving down the tree postorder (tips to root), and recursively solving the Kolmogorov backward equation of the Markov chain along each edge (Kolmogorov 1931; Feller 1949). This works because each edge is assumed to represent a realization of a continuous-time Markov chain that is independent of all other edges, with initial state equal to the final state at the parent node. The Kolmogorov backward equation is

a differential equation that describes how the likelihoods of arriving at a “target state” (the observed data) change as one moves backward in time.

In the simple case of a character-independent birth–death model, where diversification rates are either constant or depend only on time (and not on the value of an evolving state) (e.g., Morlon et al. 2011), the Kolmogorov backward equation describes the likelihood $X(t)$ that a lineage alive at “age” t (time before present) would leave exactly one descending lineage in the phylogeny at some fixed later time:

$$\frac{dX}{dt} = [2\lambda(t)E(t) - \lambda(t) - \mu(t)]X(t), \quad (1)$$

where λ is the speciation rate, μ is the extinction rate, and $E(t)$ is the probability that a lineage alive at age t would be absent from the phylogeny (computed separately). We mention that this class of models includes models where the time-dependency of λ and μ also partly stems from a dependency on varying environmental conditions (Condamine et al. 2013), as well as models where rates shift discontinuously over time (Stadler 2011a). The solution to the differential equation (1), for any given initial condition at age s , is given by the simple product:

$$X(t) = \Psi(s, t) \cdot X(s), \quad (2)$$

where the factor $\Psi(s, t)$ is given by:

$$\Psi(s, t) = e^{\int_s^t [\lambda(u) - \mu(u)] du} \cdot \frac{\left[1 + \rho \int_0^s e^{\int_0^\tau [\lambda(\sigma) - \mu(\sigma)] d\sigma} \lambda(\tau) d\tau \right]^2}{1 + \rho \int_0^t e^{\int_0^\tau [\lambda(\sigma) - \mu(\sigma)] d\sigma} \lambda(\tau) d\tau}, \quad (3)$$

and where ρ is the sampling fraction (fraction of extant species included in the tree). Observe that Eq. (2) can be used to obtain the solution to the differential equation (1) for any arbitrary initial condition, and hence the $\Psi(s, t)$ fully encode the dynamics expressed by the differential equation. The quantity $\Psi(s, t)$ must be computed for each edge in the tree, where s is the age of the child node and t is the age of the parent node (Morlon et al. 2011). We mention at this point that for any three ages t_0, s, t , the following property holds:

$$\Psi(s, t) = \Psi(t_0, t) \cdot \Psi(t_0, s)^{-1}. \quad (4)$$

Hence, if $\Psi(t_0, t)$ was known (e.g., precalculated) for some fixed t_0 and for all t , then one could calculate $\Psi(s, t)$ for any arbitrary s, t through the simple formula in Eq. (4). As we explain below, such a relationship can be retrieved for a very general class of models and constitutes the foundation of our proposed algorithm.

As mentioned above, a similar logic applies to Mk models of trait evolution (Pagel 1994), where transitions between any two states $i \rightarrow j$ occur along edges according to some fixed probability rate Q_{ij} . In Mk models, the Kolmogorov backward equation describes the evolution of the likelihoods $X_i(t)$ that a lineage, which at age t was

at state i , would have a specific state at some fixed later time:

$$\frac{d\mathbf{X}}{dt} = \mathbf{Q} \cdot \mathbf{X}, \quad (5)$$

where \mathbf{X} is a vector containing the likelihoods X_1, X_2, \dots and \mathbf{Q} is the transition rate matrix. Calculating the model's likelihood involves solving the above differential equation for each edge in the tree, in postorder traversal, with the initial conditions at each node depending on the likelihoods calculated for the child edges. At the root, the final X_i are averaged to obtain an overall likelihood for the model. For any given initial condition at age s , the solution to the differential equation (5) is given by the product:

$$\mathbf{X}(t) = \Psi(s, t) \cdot \mathbf{X}(s), \quad (6)$$

where $\Psi(s, t) = e^{(t-s)\mathbf{Q}}$ is the matrix exponential. The fact that solutions to the differential equation (5) can be expressed as matrix exponentials is sometimes used for efficient computations of model likelihoods (Louca and Doebeli 2017). As in the previous example, the matrices $\Psi(s, t)$ fully encode the dynamics expressed in the differential equation (5), and for any three ages t_0, s, t satisfy the relationship:

$$\Psi(s, t) = \Psi(t_0, t) \cdot \Psi(t_0, s)^{-1}, \quad (7)$$

where $\Psi(t_0, s)^{-1}$ is the matrix inverse.

Our final example is models where speciation and extinction rates depend on the state of an evolving discrete character. Here, and throughout the article, we focus primarily on discrete-state speciation and extinction models (BiSSE and MuSSE; Maddison et al., 2007; FitzJohn, 2012) and their extensions to including incomplete sampling (FitzJohn et al. 2009), overlapping states (GeoSSE; Goldberg et al. 2011), hidden variables (HiSSE, MuHiSSE, SecSSE, and GeoHiSSE; Beaulieu and O'Meara 2016; Caetano et al. 2018; Herrera-Alsina et al. 2019), and cladogenetic state transitions (BiSSE-ness and ClaSSE; Goldberg and Igić 2012; Magnuson-Ford and Otto 2012), henceforth collectively "dSSE". The likelihood of a dSSE model with S diversification-modulating trait states is calculated based on a set of "extinction probabilities" $E_i(t)$ and likelihoods $X_i(t)$, defined for each state $i = 1, \dots, S$ and age t . More precisely, $E_i(t)$ is the probability that a lineage, which at age t was in state i , would be absent from the phylogeny either due to eventual extinction or due to incomplete species sampling. $X_i(t)$ is the likelihood that a lineage, which at age t was in state i , would evolve into the clade observed in the given phylogeny, taking into account the present-day states at the tips (if known). The variables $E_i(t)$ and $X_i(t)$ are computed by solving a system of differential equations along each edge in backward time. For dSSE models with noncladogenetic transitions (such as BiSSE, MuSSE, SecSSE, GeoSSE, HiSSE, and GeoHiSSE), these

differential equations take the form:

$$\frac{dE_i}{dt} = \mu_i - (\lambda_i + \mu_i)E_i(t) + \lambda_i E_i(t)^2 + \sum_j Q_{ij} E_j(t), \quad (8)$$

$$\frac{dX_i}{dt} = [2\lambda_i E_i(t) - \lambda_i - \mu_i] X_i(t) + \sum_j Q_{ij} X_j(t), \quad (9)$$

where Q_{ij} is the (anagenetic) transition rate from state i to state j along a lineage, λ_i are the state-dependent speciation rates and μ_i are the state-dependent extinction rates. For models with cladogenetic transitions (BiSSE-ness and ClaSSE), the above differential equations are somewhat modified to accommodate state transitions during speciation events (e.g., see Goldberg and Igić 2012, Appendix equations A1 and A2 therein). In all dSSE models, the extinction probabilities E_i can be computed regardless of the likelihoods X_j and regardless of the tree structure, by integrating the differential equation (8) from the present all the way back to the root, with initial conditions at present ($t=0$) depending on the fraction of extant species in each state i that is included in the phylogeny ("sampling fractions"). In contrast, the X_i must be computed for each edge, traversing postorder from tips to root, with the initial conditions at each node depending on the values computed for the child edges (details in Appendix). At the root, the final X_i are averaged to obtain an overall likelihood for the model. Contrary to the previous two examples, an explicit formula for the solutions of the differential equation (9) is almost never available. As we show below, however, a relationship between solutions along different time intervals as in the previous examples (Eqs. 4 and 7) can still be retrieved.

A NEW ALGORITHM FOR THE LIKELIHOOD OF MACROEVOLUTIONARY MODELS

General Description

All of the macroevolutionary models described above, and in fact, many others, share the following fundamental aspect: Defining and computing the likelihood involves the calculation of one or more variables X_i at each node, based on a linear differential equation that must be solved in backward time along each edge:

$$\frac{d\mathbf{X}}{dt} = \mathbf{A}(t) \cdot \mathbf{X}(t), \quad (10)$$

where $\mathbf{X}(t)$ is a column-vector listing the variables $X_1(t), X_2(t), \dots$ to be computed along a specific edge and $\mathbf{A}(t)$ is some square matrix. For example, in the case of Mk models Eq. (10) corresponds to Eq. (5), and in the case of MuSSE models Eq. (10) corresponds to Eq. (9). The coefficients in the matrix $\mathbf{A}(t)$, which describes the infinitesimal transitions of \mathbf{X} along an edge, may depend on time, model parameters and the data

at hand, but must be independent of the particular edge. As explained earlier, $\mathbf{X}(t)$ typically represents the likelihoods of some given observations depending on the state of a lineage at some age t , in which case Eq. (10) is the Kolmogorov backward equation of the underlying stochastic Markov process (Kolmogorov 1931; Feller 1949) and $\mathbb{A}(t)$ depends on the instantaneous probability rates of modeled events (e.g., extinction, speciation, trait changes). The initial conditions at each node are typically specified based on the solutions of \mathbf{X} on the descending edges, in which case \mathbf{X} must be computed in a postorder fashion (from tips to root), although in some simple models a postorder traversal is not necessary (Morlon et al. 2011; Stadler 2011a; Condamine et al. 2013). For massive trees and for most models, explicitly solving the differential equation (10) for each edge can lead to impractically long computation times. Indeed, since edges (e.g., in-sister clades) span repeatedly overlapping time intervals, in large trees this approach exhibits a high level of redundancy. As explained below, this redundancy can be partly removed with an appropriately revised algorithm.

The linear structure of the differential equation (10) implies that it is in principle possible to find a general representation of solutions, such that any given initial condition at a node can be mapped to the corresponding solution at the parent node without explicitly solving the differential equation along the connecting edge. Before showing how such a representation can be obtained, it is useful to first highlight some of its general properties. For any two ages s and t , let $\Psi(s, t)$ be a function that maps initial conditions at age s to the corresponding solution of the differential equation (10) at time t ; symbolically $\Psi(s, t): \mathbf{X}(s) \mapsto \mathbf{X}(t)$. That is, for any given \mathbf{X}_1 and any age s , let $\mathbf{X}(t) = \Psi(s, t)(\mathbf{X}_1)$ be the solution to the differential equation:

$$\frac{d\mathbf{X}(t)}{dt} = \mathbb{A}(t) \cdot \mathbf{X}(t), \quad (11)$$

for the specific initial condition $\mathbf{X}(s) = \mathbf{X}_1$ (note that the solution to the differential equation depends on the initial condition). The collection of mappings $\Psi(s, t)$, which encode the correspondence of initial conditions to solutions of a differential equation, is known in the dynamical systems literature as the “flow” of the differential equation (Olver 2012; Arnold 2013). The flow thus provides an alternative and complete description of the dynamics encoded by the differential equation; instead of describing changes in infinitesimal time steps, the flow describes changes across any finite time interval $s \rightarrow t$. In the typical scenario where \mathbf{X} represents state-dependent likelihoods of observing the data, as in the examples discussed above, the flow $\Psi(s, t)$ becomes a “likelihood flow” that describes how the likelihoods \mathbf{X} are transformed between any two ages s and t . Observe that the quantities $\Psi(s, t)$ introduced for the model examples in the previous section (Eqs. 3 and 6) constituted exactly the flow of their Kolmogorov backward equations.

A defining property of flows is that for any three ages t_0, s, t , the following relationship holds:

$$\Psi(s, t)(\mathbf{X}_1) = \Psi(t_0, t)(\Psi(s, t_0)(\mathbf{X}_1)). \quad (12)$$

That is, instead of mapping the initial condition \mathbf{X}_1 at age s to the corresponding solution at age t , one can first map \mathbf{X}_1 from age s to age t_0 , and then map the obtained solution from age t_0 to age t . Since $\Psi(s, t_0)$ is the inverse of $\Psi(t_0, s)$, we obtain the representation:

$$\Psi(s, t)(\mathbf{X}_1) = \Psi(t_0, t)(\Psi(t_0, s)^{-1}(\mathbf{X}_1)). \quad (13)$$

This symbolic representation forms the foundation of our algorithm: If one could somehow precalculate the flow $\Psi(t_0, t)$ for some fixed t_0 (such as $t_0 = 0$) and for all $t > t_0$, then one could obtain solutions for any initial condition defined at any other age s through the right-hand-side of Eq. (13). Conceptually, Eq. (13) provides an alternative, more abstract, description for the progression of \mathbf{X} along edges and between nodes that is mathematically equivalent to the differential equation (10).

The precise nature of the flow Ψ depends on the nature of the differential equation (10). How, then, can one explicitly calculate the flow Ψ in practice? As the differential equation (10) is linear, for any two ages t_0 and t the function $\Psi(t_0, t)$ must itself be linear. Hence, $\Psi(t_0, t)$ can be written in matrix format, that is, the abstract notation $\Psi(t_0, t)(\mathbf{X}_0)$ becomes $\Psi(t_0, t) \cdot \mathbf{X}_0$, where $\Psi(t_0, t)$ is a matrix of the same size as \mathbb{A} . This matrix satisfies the differential equation:

$$\frac{d\Psi(t_0, t)}{dt} = \mathbb{A}(t) \cdot \Psi(t_0, t), \quad (14)$$

with initial condition $\Psi(t_0, t_0) = \mathbb{I}$, where \mathbb{I} is the identity matrix. Thus, for any initial condition $\mathbf{X}(s) = \mathbf{X}_1$ at some age s , the corresponding solution at age t can be obtained algebraically:

$$\mathbf{X}(t) = \Psi(t_0, t) \cdot \Psi(t_0, s)^{-1} \cdot \mathbf{X}_1, \quad (15)$$

where $\Psi(t_0, s)^{-1}$ is the matrix inverse. The differential equation (14) can itself be solved from the present ($t = 0$) all the way to the root ($t = t_R$), regardless of tree structure and passing only once through each time point. Typically, t_0 will simply correspond to the present, that is, $t_0 = 0$. Once $\Psi(t_0, t)$ is calculated for all t , one can calculate the solution of the differential equation (10) at one end of an edge, given any initial condition at its other end, without solving the differential equation along the edge from scratch. This idea is illustrated in Figure 1, where the flow $\Psi(t_0, t)$ is used to compute the variable \mathbf{X} at successive nodes, traversing from tips to root.

Calculating the term $\Psi(t_0, s)^{-1}$ in Eq. (15) corresponds to inverting the matrix $\Psi(t_0, s)$, which can be computationally costly and is in fact not necessary. Indeed, the entire expression $\Psi(t_0, s)^{-1} \cdot \mathbf{X}_1$ in Eq. (15) can be replaced by a vector \mathbf{X}_0 that must be chosen such

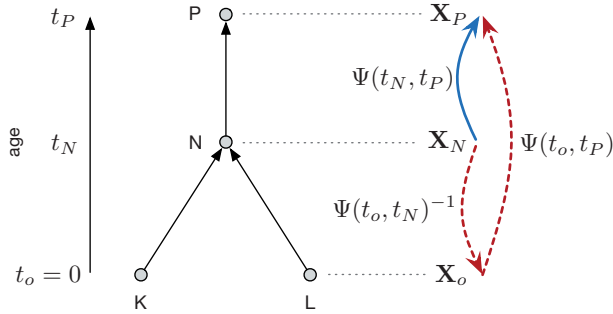


FIGURE 1. Conceptual illustration of the revised algorithm. Our proposed algorithm can be used to rapidly compute variables (e.g., state likelihoods) at nodes that are *a priori* defined as solutions of a linear differential equation along edges. In the example illustrated, as in dSSE models, the initial condition for the vector-valued variable \mathbf{X} at node N is determined based on the values of \mathbf{X} calculated previously on the descending edges (connecting tips L and K). The goal is to obtain the solution \mathbf{X}_P of the differential equation along edge $N \rightarrow P$, given the initial condition \mathbf{X}_N at node N . Instead of explicitly solving this differential equation along the edge, one can calculate \mathbf{X}_P as $\mathbf{X}_P = \Psi(t_0, t_P) \cdot \Psi(t_0, t_N)^{-1} \cdot \mathbf{X}_N$, where t_0 is some starting time point (e.g., $t_0 = 0$) for which the flow $\Psi(t_0, t)$ has been previously calculated. The direct mapping $\Psi(t_N, t_P)$ (continuous arrow) is equivalent to the product $\Psi(t_0, t_P) \cdot \Psi(t_0, t_N)^{-1}$ (dashed arrows), and hence an explicit calculation of $\Psi(t_N, t_P)$ is not necessary.

that it satisfies the condition:

$$\Psi(t_0, s) \cdot \mathbf{X}_0 = \mathbf{X}_1. \quad (16)$$

To see why this is the case, note that the vector $\mathbf{Y}(t) = \Psi(t_0, t) \cdot \mathbf{X}_0$ satisfies the differential equation

$$\frac{d\mathbf{Y}}{dt} = \frac{d\Psi(t_0, t)}{dt} \cdot \mathbf{X}_0 = \mathbb{A}(t) \cdot \Psi(t_0, t) \cdot \mathbf{X}_0 = \mathbb{A}(t) \cdot \mathbf{Y}(t), \quad (17)$$

with initial condition

$$\mathbf{Y}(s) = \Psi(t_0, s) \cdot \mathbf{X}_0 = \mathbf{X}_1, \quad (18)$$

which is the same differential equation and initial condition satisfied by $\mathbf{X}(t)$ in Eq. (15). Thus, it is not actually necessary to invert the entire matrix $\Psi(t_0, s)$, so long as a solution \mathbf{X}_0 to Eq. (16) can be found. Solving the linear system in Eq. (16) is generally easier than inverting the entire matrix $\Psi(t_0, s)$, and corresponds to mapping \mathbf{X}_1 “back to the future” at age t_0 ; the vector \mathbf{X}_0 is the hypothetical initial condition at t_0 that would lead to \mathbf{X}_1 at age s according to the differential equation (10).

Here we introduced the flow Ψ as an alternative description of the differential equation (10), which in typical macroevolutionary models specifies the instantaneous rates at which likelihoods change in backward time along edges. The flow can be seen as the “macroscopic” probabilistic behavior of the model (i.e., across the finite time steps spanning adjacent nodes), emerging from the “microscopic” behavior (i.e., across infinitesimal time steps) described by the differential equation (10). This relationship is analogous to the duality between discrete-time and continuous-time population models, where the former conceptually correspond to the time-integrated version of the latter. The flow could thus enable novel interpretations of

macroevolutionary processes and allow previously unrecognized model generalizations. For example, while every model with a Kolmogorov backward equation of the form in Eq. (10) admits a likelihood flow, the reverse need not be true. Indeed, one could envision models where anagenetic character transitions along edges occur discontinuously at discrete-time points (e.g., due to sudden environmental change); in such scenarios, the flow algorithm may be more suitable than differential equation models.

A Revised Algorithm for dSSE Models Based on “Flow”

In the following, we illustrate how our flow algorithm can be used to efficiently calculate the likelihood of dSSE models. As explained above, the flow algorithm only requires that the differential equation for the likelihoods along each edge, abstracted as in Eq. (10), is linear and has coefficients that are independent of the particular edge. This condition is satisfied for dSSE models with noncladogenetic transitions (Eq. 9) as well as for dSSE models with cladogenetic transitions (Goldberg and Igić 2012; Magnuson-Ford and Otto 2012). Note that all dSSE models are based on equations analogous to MuSSE (Eqs. 8 and 9), although they may differ in the interpretation of states, the initial conditions at the tips, the weighting of the likelihoods at each node, and how likelihoods are combined at each node; for models with cladogenetic transitions, additional terms are included in the differential equations. The flow algorithm exemplified below for MuSSE can thus also be applied to all other dSSE models mentioned above.

The algorithm begins by solving the differential equation (8) to obtain the trajectory of the extinction probabilities $E_i(t)$ from the present to the root age. For given computed E_1, \dots, E_S (where S is the number of diversification-modulating states), the differential equations for \mathbf{X} along any edge (Eq. 9) can then be written in matrix notation:

$$\frac{d\mathbf{X}}{dt} = \mathbb{A}(t) \cdot \mathbf{X}(t), \quad (19)$$

where $\mathbb{A}(t)$ is a time-dependent $S \times S$ matrix containing the various coefficients from Eq. (9). In the following, let $\mathbf{X}_N(t)$ denote the solution of Eq. (19) along the edge with child node N . The initial condition at the node, denoted $\mathbf{X}_N(t_N)$ where t_N is the node age, is specified based on the $\mathbf{X}_{C_1}(t_N), \mathbf{X}_{C_2}(t_N), \dots$ previously computed along the child edges, as in the classical formulation of MuSSE (FitzJohn 2012). At the tips, the initial conditions for X_i depend on the species sampling fractions as well as on the probability that a species in state i would have a known state, conditional upon being included in the tree (see Appendix for details).

For any age t , let $\mathbb{G}(t)$ be an $S \times S$ matrix satisfying the following differential equation:

$$\frac{d\mathbb{G}}{dt} = \mathbb{A}(t) \cdot \mathbb{G}(t), \quad (20)$$

with initial condition $\mathbb{G}(0)=\mathbb{I}$. In the terminology of the previous section, $\mathbb{G}(t)$ corresponds to the likelihood flow $\Psi(0,t)$, that is, mapping initial conditions (initial likelihoods) at age 0 to solutions of the differential equation (19) at age t . We reiterate that Eq. (20) can be solved for all $t>0$ regardless of tree structure and passing only once through each time point. Then, for any given edge connecting the parent node P (at age t_P) and child node N (at age t_N), and for any given initial condition $\mathbf{X}_N(t_N)$, one can directly compute the solution of the differential equation (19) at t_P using simple matrix algebra:

$$\mathbf{X}_N(t_P) = \mathbb{G}(t_P) \cdot \mathbf{X}_N^0, \quad (21)$$

where \mathbf{X}_N^0 is the solution to the linear system:

$$\mathbb{G}(t_N) \cdot \mathbf{X}_N^0 = \mathbf{X}_N(t_N). \quad (22)$$

Equation (22) is Eq. (16) for the special case where $t_0=0$, $s=t_N$, $\mathbf{X}_0=\mathbf{X}_N^0$, $\mathbf{X}_1=\mathbf{X}_N(t_N)$ and $\mathbb{G}(t_N)=\Psi(0,t_N)$.

Observe that, for any given edge, we have replaced the need to solve the differential equation (19) along the edge with the need to solve a system of S linear equations (Eq. 22) and performing a matrix multiplication (Eq. 21). As a tradeoff, we need to precompute $\mathbb{G}(t)$ for all ages up until the root (Eq. 20). As we demonstrate below in our simulations, for large trees this approach tends to be computationally much more efficient, despite the slight initial overhead of calculating \mathbb{G} . Indeed, the time needed to calculate \mathbb{G} scales linearly with the age span of the tree, which itself scales only sublinearly (typically logarithmically) with tree size.

We mention that the above algorithm can in principle also be extended to quantitative-trait-dependent speciation and extinction models (QuaSSE; FitzJohn 2010), by replacing the matrix-valued differential equation in Eq. (20) with a partial differential equation, and by replacing matrix multiplications as in Eq. (21) with convolution integrals. The situation, however, becomes complicated when writing the linear system in Eq. (22) in integral form, because deconvolutions tend to be hard inverse problems (Groetsch and Groetsch 1993). Discretizing the continuous trait, in order to solve these differential and integral equations numerically, essentially would lead back to the case of discrete-trait SSEs. Developing efficient algorithms for this limit of large S is undoubtedly a separate challenge.

EVALUATION AND COMPARISON TO OTHER DSSE IMPLEMENTATIONS

We implemented the above algorithm for dSSE likelihoods in the R package *castor* (Louca and Doebeli 2017), a project devoted to making phylogenetics methods accessible to modern large datasets using redesigned algorithms. Our implementation can calculate the likelihood of a model for a specific set of parameters, but can also perform maximum-likelihood estimation of model parameters and parametric

bootstrapping for estimating confidence intervals. *castor* supports an arbitrary number of states (S), missing and potentially biased information on tip states (see Appendix), incomplete and potentially biased species sampling, and an arbitrary number of concealed and observed states (when expressed in the terminology of Herrera-Alsina et al. 2019). In contrast to existing methods, *castor* fully supports trees containing multifurcations, a common issue in massive phylogenies. Further, *castor* can fit models using multiple alternative start parameters to reduce the risk of local nonglobal likelihood optima and can do so by using multiple CPU cores in parallel. For further details regarding the numerical implementation of the flow algorithm, see Supplementary Text S.1 (available on Dryad at <http://dx.doi.org/10.5061/dryad.6vm72sm>), for pseudocode see Supplementary Text S.2 available on Dryad. To confirm that our flow algorithm is correct and that our numerical implementation is accurate, we performed simulations of BiSSE models with random parameters and compared the log-likelihoods calculated for the simulated data using *castor* and another popular R package, *diversitree* (FitzJohn 2012) (Supplementary Text S.4 available on Dryad). We found that across all simulated trees the log-likelihoods were practically identical between the two methods, with relative differences always below 0.01% (Supplementary Fig. S1 available on Dryad). We also performed maximum-likelihood estimations of model parameters for simulated BiSSE and HiSSE models, and compared the resulting parameter estimates to their true (known) values, using *castor* and two other implementations: *diversitree* (BiSSE only) and *hisse* (BiSSE and HiSSE) (Beaulieu and O'Meara 2016). Using the same optimization parameters across packages, we found that parameter estimates by *castor* were generally similarly accurate as those of other tested packages, when measured in terms of the relative estimation error (Supplementary Figs. S2 and S3 available on Dryad). This was true regardless of the parameter considered (λ_i , μ_i or Q_{ij}), and regardless of tree size.

To compare the computation time of *castor* to alternative implementations we performed benchmarks with trees and tip states simulated under the BiSSE or HiSSE model with randomly chosen parameters. The following implementations were considered: *diversitree* (BiSSE only), *hisse* (BiSSE and HiSSE), and *secsse* (HiSSE only) (Herrera-Alsina et al. 2019). For each tree, we counted the time needed by each method to calculate the likelihood of the original model given the simulated data; for any given tree size, we calculated the average time needed by each method across multiple trees of that size (Figs. 2a,b details in Supplementary Text S.3 available on Dryad). As becomes evident in Figure 2a,b on large trees *castor* clearly outperforms existing implementations, reducing computation time by one or more orders of magnitude, depending on the methods compared and depending

on the size of the tree. For BiSSE, all tested methods (*castor*, *diversitree*, and *hisse*) exhibit roughly asymptotically linear scaling with tree size. Toward larger trees (>200 tips), all methods differ from each other by a roughly constant speedup factor (Fig. 2a), with *castor* being on average 12 times faster than *diversitree* and about 500 times faster than *hisse*. Toward small trees, *castor*'s run time does not converge to zero as fast as *diversitree*, and *diversitree* is somewhat faster than *castor* for trees with fewer than 200 tips. This is because for small trees *castor*'s computation time is mostly allocated to solving the differential equations for $E_i(t)$ and $G(t)$ and for preparing the interpolation of $G(t)$ for the subsequent postorder traversal. *castor*'s algorithm becomes increasingly advantageous for larger trees, where the initial preparations become less important and computation time is dominated by the postorder traversal. When compared to *diversitree* the speedup in *castor* is largely attributable to the advantages of the flow algorithm itself, whereas when compared to *hisse* the much greater performance of *castor* also partly results from *castor*'s more efficient code (as described by Louca and Doebeli 2017).

For HiSSE models, both *hisse* and *secsse* exhibit a super-linear scaling of computation times with tree size, whereas *castor* maintains linear scaling (Fig. 2b). For large trees containing hundreds of thousands of tips, *hisse* and *secsse* are about 1000–10,000 times slower than *castor*; this difference further increases for larger trees. For example, *hisse* would require about 3 h and *secsse* about 50 h for a tree with 1 million tips for a single evaluation of the likelihood function, compared to *castor* which requires about 12 s. Since *castor* treats HiSSE internally as a variant of MuSSE, its computational complexity scales similarly to BiSSE, although *castor* remains faster than *hisse* and *secsse* even for small trees. We note that the dramatic speedup of *castor* compared to *hisse* and *secsse*, when applied to HiSSE models (Fig. 2b), only partly results from the theoretical advantages of the flow algorithm. Indeed, the computation time of the original HiSSE algorithm, in which the differential equation (19) is solved along each edge, should in principle scale roughly linearly with the number of tips (assuming that the number of tips grows exponentially with the age of the clade). Hence, the super-linear scaling of *hisse*'s and *secsse*'s computation times can likely be avoided with improved code.

To exemplify the application of our implementation to real data, we investigated the diversification of angiosperms depending on their woodiness (woody vs. herbaceous), using a previously published dated tree (31,749 tips) and associated trait data (Zanne et al. 2014). We fitted a BiSSE model via maximum-likelihood, while allowing each λ_i , μ_i and Q_{ij} to differ from one another. To reduce the risk of local nonglobal likelihood maxima, fitting was repeated 20 times using random start parameters. This task took about 4 hours on our MacBook Pro laptop; the next-fastest implementation available would have taken about two days for the

same task (Fig. 2a). Estimated speciation rates were $\sim 5.1 \text{ Myr}^{-1}$ for herbaceous plants and $\sim 2.3 \text{ Myr}^{-1}$ for woody plants, with respective extinction rates almost identical to (but slightly below) speciation rates. Estimated transition rates were $\sim 0.0043 \text{ Myr}^{-1}$ from herbaceous to woody and $\sim 0.0036 \text{ Myr}^{-1}$ from woody to herbaceous, suggesting that transitions between the two growth types are rare and approximately equally likely. We note that BiSSE models do not account for temporal or geographical variations in speciation/extinction rates, previously suggested to occur in angiosperms (Jansson and Davies 2008; Crisp and Cook 2011). The present analysis should thus only serve to illustrate the application of our method to massive trees. The complete R code used is available as Supplementary Code 1 on Dryad.

EFFICIENT SIMULATION OF DSSE MODELS

An evaluation of dSSE models for large trees (e.g., Supplementary text S.5 available on Dryad), as well as complementary analyses such as parametric bootstrapping for estimating confidence intervals and Monte Carlo integration, necessitate efficient dSSE simulators for large trees, which are currently lacking. We thus also implemented an algorithm for simulating large dSSE models in forward-time, sometimes referred to as “simple sampling approach” (Stadler 2011b) (pseudocode in Supplementary text S.6 available on Dryad). Our implementation is orders of magnitude faster than any existing implementation and can handle both anagenetic and cladogenetic transitions between states, thus covering the broad range of dSSE models discussed. In our tests, *castor* was able to generate BiSSE trees with millions of tips in about 5 s (Fig. 2c, details in Supplementary text S.7 available on Dryad). When assessed over varying tree sizes, it becomes apparent that our algorithm exhibits a nearly linear scaling of computation time (power-law exponent 1.1). In contrast, *diversitree* and *hisse* (to our knowledge the only other R packages able to simulate dSSE models) both exhibit super-linear scaling (exponents 2.0 and 1.5, respectively), and would require 10–100 h to generate a tree with 1 million tips (Fig. 2c). Even when compared to existing simulators of simple uniform time-homogeneous birth–death processes, that is, ignoring trait evolution and assuming a single constant λ and μ , *castor*'s simulations of the more general BiSSE process are at least an order of magnitude faster than other tools (Supplementary Fig. S4 available on Dryad). For example, to generate a tree with 1 million tips under the simple birth–death model, and based on the fitted scaling exponents, we estimate that the package *geiger* (Pennell et al. 2014) would take on average about 73 h, the package *TESS* (Höhna et al. 2015) about 7 h, the package *phytools* (Revell 2012) about 32 h, and the package *TreeSim* (Stadler 2011b) about 112 h (although we caution the reader that *TreeSim* and *TESS* use a different conditioning and thus do not sample from the same exact distribution as *castor*; Stadler

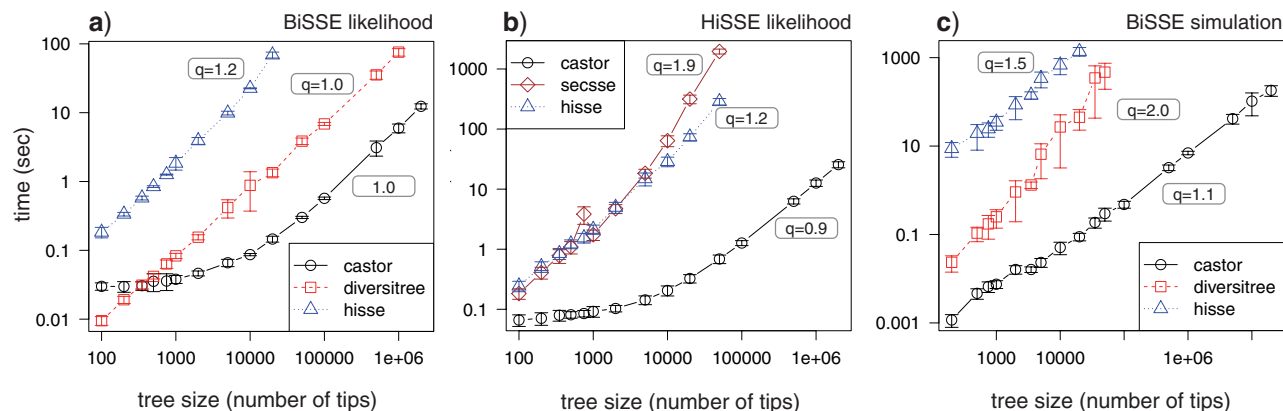


FIGURE 2. Comparison of computation times. Comparison of computation times needed for the calculation of a single BiSSE likelihood (a), the calculation of a single HiSSE likelihood (b), and the simulation of a single BiSSE model (c), using *castor* and other software packages (time T over tree size S , one curve per package). Note the logarithmic axes in all figures. Package names are listed in the legends. Fitted asymptotic power-law exponents ($T \propto S^q$) are shown next to every curve. Vertical bars show standard deviations around the mean. Compared packages include *diversitree* (FitzJohn 2012), *hisse* (Beaulieu and O'Meara 2016), and *secsse* (Herrera-Alsina et al. 2019). Detailed functions and options used are explained in the Supplemental Material.

2011b). The correctness of our code is confirmed by comparing the distribution of generated trees to those generated by *diversitree*, both in terms of their lineages-through-time curves as well as the distribution of pairwise node-to-node distances (Supplementary Text S.8 and Fig. S5 available on Dryad).

Similarly to most previous implementations, our implementation is essentially a Gillespie algorithm, which generates statistically correctly distributed trajectories of the stochastic model (Gillespie 1977). In Gillespie algorithms, the waiting time until the next event—in our case speciation, extinction, or transition between states—is randomly drawn from an exponential distribution according to the rates of the various processes. Variants of the Gillespie algorithm are also used in other implementations, such as *diversitree*, *hisse*, *phytools*, and *geiger*. The greater efficiency of our implementation is achieved in mainly two ways. First, we use temporary auxiliary redundant data structures, which are either generated at the beginning (in linear time) or continuously updated after each event (in constant time), to accelerate certain operations and eliminate redundant calculations. This enables us to achieve the linear scaling that is theoretically predicted for the Gillespie algorithm. For example, during a simulation, we keep track of lineages that are not yet extinct and in a particular state using continuously updated lookup tables (Louca and Doebeli 2017); hence, choosing the next tip for a speciation/extinction/transition event can be done in constant time. Indeed, a common issue that we observed in other implementations is the repeated use of function calls (such as the R function *which*) that iterate through the entire tree at each event, thus leading to a needless super-linear scaling of overall computation time. Second, our code is almost entirely written in C++, a programming language that is especially well suited for high-performance computing. Note that the algorithms underlying *TreeSim* and *TESS* should, in theory, also

scale linearly with tree size and should be comparable (if not faster) than the Gillespie algorithm, since they sample only branching times in the extant phylogeny rather than all speciation/extinction events (Stadler 2011b; Höhna et al. 2015). The lower performance and super-quadratic scaling of *TreeSim* and *TESS* (power-law exponent ~ 2.2) thus likely result from suboptimal code design, and could perhaps be improved using similar approaches as in *castor* (Louca and Doebeli 2017).

CONCLUSIONS

An impressive number of mathematical methods have been developed for comparative phylogenetics over the last few decades (O'Meara 2012; Pennell and Harmon 2013; Garamszegi 2014; Morlon 2014; Ng and Smith 2014; Harmon 2018). However, existing numerical procedures for the majority of these methods—while adequate in the past—scale poorly to increasingly common large-scale phylogenies. As biology ventures into an era of massive data sets, and bottlenecks become increasingly computational, a deeper consideration of algorithmic complexity and numerical limitations is needed in order to keep these mathematical tools applicable (Freckleton 2012; Tung Ho and Ané 2014; Goolsby 2017; Louca and Doebeli 2017).

Here, we present a new algorithm for calculating the likelihood of a large set of macroevolutionary models, including diversification models with time-dependent speciation and extinction rates (Morlon et al. 2011; Condamine et al. 2013; Rabosky 2014), models for discrete-state-dependent diversification (Maddison et al. 2007; FitzJohn et al. 2009; Rabosky and Glor 2010; Goldberg et al. 2011; FitzJohn 2012; Goldberg and Igić 2012; Magnuson-Ford and Otto 2012; Beaulieu and O'Meara 2016; Caetano et al. 2018; Herrera-Alsina et al. 2019) and Mk models for the evolution of a discrete trait along a fixed tree (Pagel 1994; Lewis 2001). Our

algorithm makes use of the fact that the solutions to the Kolmogorov backward equation, a cornerstone of the aforementioned models, can be represented by a likelihood flow that only needs to be computed once from the present to the root. Our flow algorithm can also be applied to dSSE models where the rates λ_i , μ_i , and Q_{ij} depend on time and/or on time-dependent environmental variables (Rabosky and Glor 2010), as well as to Mk models with time-dependent transition rates. The algorithm can even be applied to cases where rate parameters vary between some taxa (Alfaro et al. 2009; Rabosky 2014), so long as a separate flow is used for each taxon-specific rate class. The flow algorithm has the potential to substantially reduce computation time whenever it is costly to solve the Kolmogorov backward differential equation for the likelihoods, as is typically the case for complex models for which no closed-form solutions are known.

Our tests showed that for large trees our algorithm, which we used to newly implement various previous dSSE models, is one or more orders of magnitude faster than existing implementations. For maximum-likelihood estimation or Bayesian Markov Chain Monte Carlo, which can involve thousands of evaluations of the likelihood function and take hundreds of hours, these differences in performance become crucial determinants of the feasibility of a study. We also presented a new numerical method for simulating dSSE models, which for large trees is several orders of magnitude faster than existing methods. Our methods are provided through *castor*, an R package for efficient comparative phylogenetics on large trees (Louca and Doebeli 2017). Practically, our methods make a large class of diversification models accessible to modern massive phylogenies, which are bound to shed new light on macroevolutionary questions. We also hope that our algorithm gives researchers a new perspective on macroevolutionary models and, in doing so, helps spur the advance of the next-generation of comparative methods.

SUPPLEMENTARY MATERIAL

Data available from the Dryad Digital Repository: <http://dx.doi.org/10.5061/dryad.6vm72sm>.

CODE AVAILABILITY

Methods described in this article for dSSE models are available in the R package *castor*, as functions `fit_musse` and `simulate_musse`. The package *castor* is available on the Comprehensive R Archive Network (CRAN).

FUNDING

This work was supported by a startup grant by the University of Oregon, USA [to S.L.] and Natural Sciences

and Engineering Research Council of Canada (NSERC) Discovery Grant [to M.W.P.].

AUTHOR CONTRIBUTIONS

S.L. and M.W.P. conceptualized the project. S.L. conceived the flow algorithm and wrote the computer code. Both authors contributed to the writing of the manuscript.

APPENDIX

AN EXTENSION TO EXISTING DSSE MODELS

In the following, we describe how existing dSSE models can be extended to account for multifurcations in the phylogeny (a common issue in massive phylogenies), as well as for potential biases in the identification of tip states, that is, where some states are easier to detect/confirm than others. Such “reveal biases” are probably present in a multitude of traits, for example when it is easier to confirm the presence of a behavioral trait or metabolic capability than its absence. A prominent example are bacterial metabolic phenotypes, where culturing success is strongly biased toward specific phenotypes, depending on available techniques and current research interests (Dunbar et al. 1997; Marchesi and Weightman 2003; Tamaki et al. 2005; Lagkouravdos et al. 2017). Existing formulations of dSSE ignore such biases, that is, it has so far been assumed that either all tips have known state (Maddison et al. 2007), or that all tip states have the same probability of being known (FitzJohn et al. 2009; FitzJohn 2012; Beaulieu and O’Meara 2016; Herrera-Alsina et al. 2019).

In dSSE, available trait data and information about sampling fractions is incorporated into a model’s likelihood via the initial conditions assumed for the E_i (probability that a lineage at state i will eventually be absent from the tree) and the likelihoods X_i at the tips, that is, at age $t=0$. Specifically, the initial conditions for E_i at $t=0$ depend on the fraction of extant species in state i that is included in the phylogeny, usually referred to as “sampling fraction” and denoted ρ_i :

$$E_i(0) = 1 - \rho_i. \quad (\text{A.1})$$

The initial condition for X_i at $t=0$ is defined separately for each tip, and depends on the sampling fraction of species in state i , as well as on the probability that a species in state i would have a known (“revealed”) state, conditional upon being included in the tree. In existing dSSE variants, this probability—here referred to as “reveal fraction” r_i —was assumed to be independent of state (Maddison et al. 2007; FitzJohn et al. 2009; FitzJohn 2012; Beaulieu and O’Meara 2016; Herrera-Alsina et al. 2019). For tips known to be in state i , thus:

$$X_i(0) = \rho_i \cdot r_i, \quad X_j(0) = 0 \quad \forall j \neq i, \quad (\text{A.2})$$

and for tips with unknown state:

$$X_j(0) = \rho_j \cdot (1 - r_j) \quad \forall j. \quad (\text{A.3})$$

Observe that even if the state of a tip is unknown, the mere fact that it is included in the phylogeny (which occurs with probability ρ_i) and the fact that its state is unknown (which occurs with probability $1 - r_i$), constitute potential information that is incorporated into the model's likelihood. In [Supplementary Text S.9](#) available on Dryad, we use simulations to illustrate how ignoring or accounting for reveal biases can influence dSSE parameter estimates. Note that, unless most other model parameters are known *a priori*, it may not be possible to estimate the reveal fractions r_i from the phylogenetic data alone. For example, for trait-independent birth–death models it is well known that the sampling fraction ρ cannot be directly estimated from the tree when the speciation and extinction rates are unknown ([Stadler 2009](#); [Morlon et al. 2010](#); [Stadler and Steel 2019](#)), and that ρ must be determined using additional information (e.g., via mark-recapture-type surveys, [Louca et al., 2018](#)). It is thus possible that the r_i may also need to be determined beforehand using additional data, although more thorough investigations of parameter identifiability are required to confirm this suspicion.

At internal nodes, the initial conditions for \mathbf{X} depend on the values computed for the descending clades, as explained in the following. Since we will be referring to the values of \mathbf{X} at various nodes, in the following we will deploy double-indices, with $X_{N,j}$ denoting the value of the j -th component of \mathbf{X} (where $j = 1, \dots, S$) at node N , and with \mathcal{N} denoting the set of all nodes (hence $N \in \mathcal{N}$). At any node $N \in \mathcal{N}$ of age t_N and having child nodes $C_1, \dots, C_n \in \mathcal{N}$ (with $n = 2$ in the case of bifurcating trees), the initial condition $X_{N,i}(t_N)$ is determined by the final values of $X_{C_1,i}, \dots, X_{C_n,i}$ on the daughter lineages:

$$X_{N,i}(t_N) = \lambda_i^{n-1} \prod_{k=1}^n X_{C_k,i}(t_N). \quad (\text{A.4})$$

Note that classical formulations of dSSE only consider the bifurcating case ($n = 2$). The more general scaling factor λ_i^{n-1} for any $n \geq 2$ can be derived in two alternative ways. First, multifurcations can be decomposed into $n - 1$ bifurcating sub-nodes in close temporal proximity, that is, with the length of artificially introduced edges being infinitesimally small. Along these edges, the likelihoods \mathbf{X} change only little, and at each subnode a factor λ_i would be introduced as one traverses toward the root; the classical formula for dSSE in bifurcating trees would thus eventually lead to the expression in Eq. (A.4) for the likelihoods at the subnode closest to the root. Second, the scaling λ_i^{n-1} corresponds to the leading-order expression for the probability that the cladogenic process generates n lineages during an infinitesimal time step ε , after rescaling to remove time units. Indeed, for a cladogenic process with some speciation rate λ_i and

extinction rate μ_i , starting with a single lineage at time t , the probability of having n or more extant lineages at time $t + \varepsilon$ is given by ([Nee et al. 1994](#)):

$$P(\varepsilon) = \sum_{k=n}^{\infty} \frac{\delta_i}{\lambda_i - \mu_i e^{-\delta_i \varepsilon}} \cdot [1 - u_\varepsilon] u_\varepsilon^{k-n-1}, \quad (\text{A.5})$$

where $\delta_i = \lambda_i - \mu_i$ and where:

$$u_\varepsilon := \lambda_i \frac{1 - e^{-\delta_i \varepsilon}}{\lambda_i - \mu_i e^{-\delta_i \varepsilon}}. \quad (\text{A.6})$$

Keeping only terms of leading order in ε yields:

$$P(\varepsilon) = \varepsilon^{n-1} \lambda_i^{n-1} + \mathcal{O}(\varepsilon^n), \quad (\text{A.7})$$

and hence one recovers the scaling factor in Eq. (A.4).

We clarify that Eq. (A.4) is primarily designed to deal with poorly resolved multifurcations, that is, where multiple bifurcations occurred in such close temporal proximity that they cannot be resolved in the phylogeny. As most existing phylogenetic software (including most existing implementations of dSSE) crash when applied to multifurcating trees, it is common practice to artificially resolve multifurcations into multiple and closely adjacent bifurcations (i.e., by introducing short artificial edges), prior to applying dSSE. Our formula essentially allows directly calculating the outcome of such an adjustment without actually modifying the input tree, in the mathematical limit where the introduced artificial edges are infinitesimally small. Note that Eq. (A.4) does not apply to truly multifurcating diversification models, that is, where true n -furcations occur at some nonzero probability rate.

REFERENCES

- Alfaro M.E., Santini F., Brock C., Alamillo H., Dornburg A., Rabosky D.L., Carnevale G., Harmon L.J. 2009. Nine exceptional radiations plus high turnover explain species diversity in jawed vertebrates. *Proc. Natl. Acad. Sci. USA*. 106:13410–13414.
- Arnold L. 2013. *Random dynamical systems*. Springer Monographs in Mathematics. New York: Springer Berlin Heidelberg.
- Beaulieu J.M., O'Meara B.C. 2016. Detecting hidden diversification shifts in models of trait-dependent speciation and extinction. *Syst. Biol.* 65:583–601.
- Caetano D.S., O'Meara B.C., Beaulieu J.M. 2018. Hidden state models improve state-dependent diversification approaches, including biogeographical models. *Evolution*. 72:2308–2324.
- Cantalapiedra J.L., FitzJohn R.G., Kuhn T.S., Fernández M.H., DeMiguel D., Azanza B., Morales J., Mooers A.Ø. 2014. Dietary innovations spurred the diversification of ruminants during the Cenozoic. *Proc. R. Soc.* 281:20132746.
- Condamine F.L., Rolland J., Morlon H. 2013. Macroevolutionary perspectives to environmental change. *Ecol. Lett.* 16:72–85.
- Cornwell W.K., Pearse W.D., Dalrymple R.L., Zanne A.E. 2019. What we (don't) know about global plant diversity. *Ecography*. doi: 10.1111/ecog.04481.
- Crisp M.D., Cook L.G. 2011. Cenozoic extinctions account for the low diversity of extant gymnosperms compared with angiosperms. *New Phytologist*. 192:997–1009.
- David L.A., Alm E.J. 2011. Rapid evolutionary innovation during an Archaean genetic expansion. *Nature*. 469:93–96.

- Dunbar J., White S., Forney L. 1997. Genetic diversity through the looking glass: effect of enrichment bias. *Appl. Environ. Microbiol.* 63:1326–1331.
- Etienne R.S., Haegeman B. 2012. A conceptual and statistical framework for adaptive radiations with a key role for diversity dependence. *Am. Nat.* 180:E75–E89.
- Feller W. 1949. On the theory of stochastic processes, with particular reference to applications. *Proceedings of the First Berkeley Symposium on Mathematical Statistics and Probability*. Berkeley (CA): University of California Press. 403–432 pp.
- FitzJohn R.G. 2010. Quantitative traits and diversification. *Syst. Biol.* 59:619–633.
- FitzJohn R.G. 2012. Diversitree: comparative phylogenetic analyses of diversification in R. *Meth. Ecol. Evol.* 3:1084–1092.
- FitzJohn R.G., Maddison W.P., Otto S.P. 2009. Estimating trait-dependent speciation and extinction rates from incompletely resolved phylogenies. *Syst. Biol.* 58:595–611.
- Freckleton R.P. 2012. Fast likelihood calculations for comparative analyses. *Meth. Ecol. Evol.* 3:940–947.
- Garamszegi L.Z. 2014. *Modern phylogenetic comparative methods and their application in evolutionary biology: concepts and practice*. Berlin, Heidelberg: Springer.
- Gillespie D.T. 1977. Exact stochastic simulation of coupled chemical reactions. *J. Phys. Chem.* 81:2340–2361.
- Goldberg E.E., Igić B. 2012. Tempo and mode in plant breeding system evolution. *Evolution*. 66:3701–3709.
- Goldberg E.E., Lancaster L.T., Ree R.H. 2011. Phylogenetic inference of reciprocal effects between geographic range evolution and diversification. *Syst. Biol.* 60:451–465.
- Goolsby E.W. 2017. Rapid maximum likelihood ancestral state reconstruction of continuous characters: a rerooting-free algorithm. *Ecol. Evol.* 7:2791–2797.
- Groetsch C.W., Groetsch C. 1993. *Inverse problems in the mathematical sciences*. Vol. 52. Wiesbaden: Springer.
- Harmon L.J. 2018. Phylogenetic comparative methods: learning from trees. Self published under a CC-BY-4.0 license. <https://lukejharmon.github.io/pcm/>.
- Hehemann J.H., Arevalo P., Datta M.S., Yu X., Corzett C.H., Henschel A., Preheim S.P., Timberlake S., Alm E.J., Polz M.F. 2016. Adaptive radiation by waves of gene transfer leads to fine-scale resource partitioning in marine microbes. *Nat. Commun.* 7:12860 EP.
- Henao Diaz L.F., Harmon L.J., Sugawara M.T.C., Miller E.T., Pennell M.W. 2019. Macroevolutionary diversification rates show time dependency. *Proc. Natl. Acad. Sci. USA*. 116:7403.
- Hinchliff C.E., Smith S.A., Allman J.F., Burleigh J.G., Chaudhary R., Coghill L.M., Crandall K.A., Deng J., Drew B.T., Gazis R., Gude K., Hibbett D.S., Katz L.A., Laughinghouse H.D., McTavish E.J., Midford P.E., Owen C.L., Ree R.H., Rees J.A., Soltis D.E., Williams T., Cranston K.A. 2015. Synthesis of phylogeny and taxonomy into a comprehensive tree of life. *Proc. Natl. Acad. Sci. USA*. 112:12764–12769.
- Höhna S., May M.R., Moore B.R. 2015. TESS: an R package for efficiently simulating phylogenetic trees and performing Bayesian inference of lineage diversification rates. *Bioinformatics*. 32:789–791.
- Jansson R., Davies T.J. 2008. Global variation in diversification rates of flowering plants: energy vs. climate change. *Ecol. Lett.* 11: 173–183.
- Jetz W., Thomas G., Joy J., Hartmann K., Mooers A. 2012. The global diversity of birds in space and time. *Nature*. 491:444.
- Kendall D.G. 1948. On some modes of population growth leading to RA Fisher's logarithmic series distribution. *Biometrika*. 35:6–15.
- Kolmogorov A. 1931. Über die analytischen Methoden in der Wahrscheinlichkeitsrechnung. *Math. Ann.* 104:415–458.
- Lagkouvardos I., Overmann J., Clavel T. 2017. Cultured microbes represent a substantial fraction of the human and mouse gut microbiota. *Gut Microbes*. 8:493–503.
- Larsen B.B., Miller E.C., Rhodes M.K., Wiens J.J. 2017. Inordinate fondness multiplied and redistributed: the number of species on Earth and the new pie of life. *Q. Rev. Biol.* 92:229–265.
- Latysheva N., Junker V.L., Palmer W.J., Codd G.A., Barker D. 2012. The evolution of nitrogen fixation in cyanobacteria. *Bioinformatics*. 28:603–606.
- Lewis P.O. 2001. A likelihood approach to estimating phylogeny from discrete morphological character data. *Syst. Biol.* 50:913–925.
- Louca S., Doebeli M. 2017. Efficient comparative phylogenetics on large trees. *Bioinformatics*. 34:1053–1055.
- Louca S., Shih P.M., Pennell M.W., Fischer W.W., Parfrey L.W., Doebeli M. 2018. Bacterial diversification through geological time. *Nat. Ecol. Evol.* 2:1458–1467.
- Maddison W.P., Midford P.E., Otto S.P., Oakley T. 2007. Estimating a binary character's effect on speciation and extinction. *Syst. Biol.* 56:701–710.
- Magallon S., Sanderson M.J. 2001. Absolute diversification rates in angiosperm clades. *Evolution*. 55:1762–1780.
- Magnuson-Ford K., Otto S.P. 2012. Linking the investigations of character evolution and species diversification. *Am. Nat.* 180:225–245.
- Marchesi J.R., Weightman A.J. 2003. Comparing the dehalogenase gene pool in cultivated α -halocarboxylic acid-degrading bacteria with the environmental metagenome pool. *Appl. Environ. Microbiol.* 69:4375–4382.
- Meiss J. 2007. *Differential dynamical systems*. Number v. 1 in *Monographs on Mathematical Modeling and Computation*. Philadelphia (PA): Society for Industrial and Applied Mathematics.
- Mendler K., Chen H., Parks D.H., Lobb B., Hug L.A., Doxey A.C. 2019. AnnoTree: visualization and exploration of a functionally annotated microbial tree of life. *Nucleic Acids Res.* 47:4442–4448.
- Mooers A.O., Heard S.B. 1997. Inferring evolutionary process from phylogenetic tree shape. *Q. Rev. Biol.* 72:31–54.
- Mora C., Tittensor D.P., Adl S., Simpson A.G., Worm B. 2011. How many species are there on Earth and in the ocean? *PLoS Biol.* 9: e1001127.
- Morlon H. 2014. Phylogenetic approaches for studying diversification. *Ecol. Lett.* 17:508–525.
- Morlon H., Parsons T.L., Plotkin J.B. 2011. Reconciling molecular phylogenies with the fossil record. *Proc. Natl. Acad. Sci. USA*. 108:16327–16332.
- Morlon H., Potts M.D., Plotkin J.B. 2010. Inferring the dynamics of diversification: a coalescent approach. *PLoS Biol.* 8:e1000493.
- Nee S., May R.M., Harvey P.H. 1994. The reconstructed evolutionary process. *Philos. Trans. Royal Soc. B*. 344:305–311.
- Ng J., Smith S.D. 2014. How traits shape trees: new approaches for detecting character state-dependent lineage diversification. *J. Evol. Biol.* 27:2035–2045.
- Olver P.J. 2012. *Applications of lie groups to differential equations*. Graduate Texts in Mathematics. New York: Springer.
- O'Meara B.C. 2012. Evolutionary inferences from phylogenies: a review of methods. *Annu. Rev. Ecol. Syst.* 43:267–285.
- Pagel M. 1994. Detecting correlated evolution on phylogenies: a general method for the comparative analysis of discrete characters. *Proc. R. Soc. Lond.* 255:37–45.
- Parks D.H., Chuvochina M., Waite D.W., Rinke C., Skarshewski A., Chaumeil P.A., Hugenholtz P. 2018. A standardized bacterial taxonomy based on genome phylogeny substantially revises the tree of life. *Nat. Biotechnol.* 36:996–1004.
- Pennell M.W., Eastman J.M., Slater G.J., Brown J.W., Uyeda J.C., FitzJohn R.G., Alfaro M.E., Harmon L.J. 2014. geiger v2. 0: an expanded suite of methods for fitting macroevolutionary models to phylogenetic trees. *Bioinformatics*. 30:2216–2218.
- Pennell M.W., Harmon L.J. 2013. An integrative view of phylogenetic comparative methods: connections to population genetics, community ecology, and paleobiology. *Ann. N. Y. Acad. Sci.* 1289: 90–105.
- Polz M.F., Alm E.J., Hanage W.P. 2013. Horizontal gene transfer and the evolution of bacterial and archaeal population structure. *Trends Genet.* 29:170–175.
- Rabosky D.L. 2014. Automatic detection of key innovations, rate shifts, and diversity-dependence on phylogenetic trees. *PLoS One*. 9: 1–15.
- Rabosky D.L., Donnellan S.C., Talaba A.L., Lovette I.J. 2007. Exceptional among-lineage variation in diversification rates during the radiation of Australia's most diverse vertebrate clade. *Proc. R. Soc. Lon.* 274:2915–2923.
- Rabosky D.L., Glor R.E. 2010. Equilibrium speciation dynamics in a model adaptive radiation of island lizards. *Proc. Natl. Acad. Sci. USA*. 107:22178–22183.

- Raup D.M. 1985. Mathematical models of cladogenesis. *Paleobiology*. 11:42–52.
- Revell L.J. 2012. phytools: an R package for phylogenetic comparative biology (and other things). *Methods Ecol. Evol.* 3:217–223.
- Schluter D., Pennell M.W. 2017. Speciation gradients and the distribution of biodiversity. *Nature*. 546:48.
- Smith S.A., Brown J.W. 2018. Constructing a broadly inclusive seed plant phylogeny. *Am. J. Bot.* 105:302–314.
- Stadler T. 2009. On incomplete sampling under birth–death models and connections to the sampling-based coalescent. *J. Theor. Biol.* 261:58–66.
- Stadler T. 2011a. Mammalian phylogeny reveals recent diversification rate shifts. *Proc. Natl. Acad. Sci. USA*. 108:6187–6192.
- Stadler T. 2011b. Simulating trees with a fixed number of extant species. *Syst. Biol.* 60:676–684.
- Stadler T., Steel M. 2019. Swapping birth and death: Symmetries and transformations in phylodynamic models. *Syst. Biol.* 68: 852–858.
- Tamaki H., Sekiguchi Y., Hanada S., Nakamura K., Nomura N., Matsumura M., Kamagata Y. 2005. Comparative analysis of bacterial diversity in freshwater sediment of a shallow eutrophic lake by molecular and improved cultivation-based techniques. *Appl. Environ. Microbiol.* 71:2162–2169.
- Thompson L.R., Sanders J.G., McDonald D., Amir A., Ladau J., Locey K.J., Prill R.J., Tripathi A., Gibbons S.M., Ackermann G., Navas-Molina J.A., Janssen S., Kopylova E., Vázquez-Baeza Y., González A., Morton J.T., Mirarab S., Zech X.Z., Jiang L., Haroon M.F., Kanbar J., Zhu Q., Jin S.S., Kosciółek T., Bokulich N.A., Lefler J., Brislawn C.J., Humphrey G., Owens S.M., Hampton-Marcell J., Berg-lyons D., McKenzie V., Fierer N., Fuhrman J.A., Clauset A., Stevens R.L., Shade A., Pollard K.S., Goodwin K.D., Jansson J.K., Gilbert J.A., Knight R., The Earth Microbiome Project Consortium 2017. A communal catalogue reveals earth's multiscale microbial diversity. *Nature*. 551:457–463.
- Tung Ho L.S., Ané C. 2014. A linear-time algorithm for Gaussian and non-Gaussian trait evolution models. *Syst. Biol.* 63:397–408.
- Herrera-Alsina L., van Els P., Etienne R.S. 2019. Detecting the dependence of diversification on multiple traits from phylogenetic trees and trait data. *Syst. Biol.* 68:317–328.
- Wiens J.J. 2017. What explains patterns of biodiversity across the tree of life? new research is revealing the causes of the dramatic variation in species numbers across branches of the tree of life. *BioEssays*. 39:1600128.
- Zanne A.E., Tank D.C., Cornwell W.K., Eastman J.M., Smith S.A., FitzJohn R.G., McGlinn D.J., O'Meara B.C., Moles A.T., Reich P.B., Royer D.L., Soltis D.E., Stevens P.F., Westoby M., Wright I.J., Aarssen L., Bertin R.I., Calaminus A., Govaerts R., Hemmings F., Leishman M.R., Oleksyn J., Soltis P.S., Swenson N.G., Warman L., Beaulieu J.M. 2014. Three keys to the radiation of angiosperms into freezing environments. *Nature*. 506:89–92.